

# Crystal structure and lattice dynamics of $\text{AlB}_2$ under pressure and implications for $\text{MgB}_2$

I. Loa,\* K. Kunc,<sup>†</sup> and K. Syassen

*Max-Planck-Institut für Festkörperforschung, Heisenbergstrasse 1, D-70569 Stuttgart, Germany*

P. Bouvier

*European Synchrotron Radiation Facility, BP 220, F-38043 Grenoble, France*

(Dated: November 26, 2024)

The effect of high pressures to 40 GPa on the crystal structure and lattice dynamics of  $\text{AlB}_2$  was studied by synchrotron x-ray powder diffraction, Raman spectroscopy, and first-principles calculations. There are no indications for a pressure-induced structural phase transition. The Raman spectra of the metallic sample exhibit a well-defined peak near  $980 \text{ cm}^{-1}$  at 0 GPa which can be attributed to the Raman-active  $E_{2g}$  zone-center phonon. Al deficiency of  $\sim 11\%$  in  $\text{AlB}_2$ , as indicated by the x-ray data, changes qualitatively the electronic structure, and there are indications that it may have a sizable effect on the pressure dependence of the  $E_{2g}$  phonon frequency. Similar changes of the pressure dependence of phonon frequencies, caused by non-stoichiometry, are proposed as an explanation for the unusually large variation of the pressure dependence of  $T_c$  for different samples of  $\text{MgB}_2$ .

PACS numbers: PACS: 63.20.-e, 74.25.Kc, 78.30.-j, 71.15.Nc, 62.50.+p

## I. INTRODUCTION

The  $\text{AlB}_2$  structure type and derivatives thereof are among the most frequently occurring ones for intermetallic binary and ternary compounds.<sup>1,2</sup> Transition metal diborides, belonging to this family, have been studied in some detail because of their potential application in electronic devices<sup>3</sup> to overcome current problems of electromigration, corrosion, and diffusion into the semiconductor substrate. The largest interest, however, has undoubtedly received the recently discovered superconductor  $\text{MgB}_2$  which also crystallizes in the simple  $\text{AlB}_2$  structure depicted in Fig. 1.

$\text{AlB}_2$ -type compounds have not been studied systematically at high pressures. There seem to exist no confirmed reports on pressure-induced structural phase transitions in metal diborides. There are, however, structural studies of the rare-earth metal digallides  $\text{GdGa}_2$ ,  $\text{HoGa}_2$ ,  $\text{ErGa}_2$ , and  $\text{TmGa}_2$  at high pressures.<sup>4,5,6,7</sup> With the lighter rare earth elements La—Er the digallides crystallize in the  $\text{AlB}_2$  structure at ambient pressure. In essence, all of the rare-earth metal digallides studied so far show a transition to the  $\text{UHg}_2$  structure which is isotypic to  $\text{AlB}_2$  but with a lower  $c/a$  ratio.

The superconductor  $\text{MgB}_2$  was studied at high pressures with regard to its superconducting transition temperature,<sup>8,9,10,11,12,13</sup> crystal structure,<sup>14,15,16,17,18</sup> and lattice dynamics.<sup>17,19</sup> The pressure dependence of  $T_c$  could well be explained in the framework of phonon-mediated, i.e. BCS, superconductivity.<sup>14,20,21</sup> An isostructural transition near 30 GPa was reported<sup>22</sup> but could not be reproduced in another study up to 40 GPa.<sup>18</sup> Much higher pressures may be necessary to induce transitions possibly towards the  $\text{UHg}_2$  structure.

We study here the effect of hydrostatic pressure on the crystal structure and lattice dynamics of  $\text{AlB}_2$ . Syn-

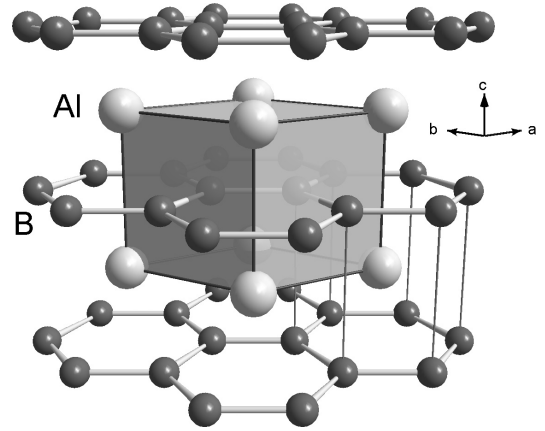


FIG. 1: Crystal structure of  $\text{AlB}_2$ . The boron atoms form honeycomb layers. Al atoms are located at the centers of hexagonal prisms that are formed by the B sheets.

chrotron x-ray powder diffraction and Raman scattering experiments are complemented by first-principles calculations. The present high-pressure study was in part motivated by the question whether some of the unusual physical properties of  $\text{MgB}_2$  – such as the sizable anharmonicity<sup>19,23,24</sup> or the remarkably large calculated pressure dependence<sup>19</sup> of the  $E_{2g}$  phonon – are specific to  $\text{MgB}_2$  or whether they are characteristic of other  $\text{AlB}_2$ -type metal diborides as well. It aims at providing high-pressure structural and lattice dynamical information for comparison with corresponding data on  $\text{MgB}_2$ . Finally, Al deficiency appears to be hardly avoidable in the growth of  $\text{AlB}_2$ .<sup>25,26</sup> We show that it has significant effect on the electronic structure of  $\text{AlB}_2$  and may also influence its lattice dynamics. We will discuss possible consequences of metal deficiency for the superconductor

MgB<sub>2</sub> where this issue is also of relevance.

## II. EXPERIMENTS

### A. Experimental Details

The structural properties of AlB<sub>2</sub> under pressure were studied up to 40 GPa by monochromatic ( $\lambda = 0.3738 \text{ \AA}$ ) x-ray powder diffraction at the European Synchrotron Radiation Facility (ESRF Grenoble, beamline ID30). Commercially available AlB<sub>2</sub> powder (Alfa Aesar, 99%) was placed in a diamond anvil cell (DAC) for pressure generation. Nitrogen was employed as a pressure medium to provide nearly hydrostatic conditions. Diffraction patterns were recorded on image plates and then integrated<sup>27</sup> to yield intensity vs.  $2\theta$  diagrams.

Raman spectra of AlB<sub>2</sub> up to 25 GPa (DAC, 4:1 methanol/ethanol mixture as a pressure medium) were excited at 633 nm utilizing a long-distance microscope objective. They were recorded in back-scattering geometry using a single-grating spectrometer with a multi-channel CCD detector and a holographic notch filter for suppression of the laser line (Dilor Labram). For the Raman experiments the DAC was equipped with synthetic diamonds (Sumitomo type IIa) which emit only minimal luminescence. In all experiments pressures were measured with the ruby luminescence method.<sup>28</sup>

### B. X-ray diffraction under pressure

Figure 2 shows x-ray diffraction patterns of AlB<sub>2</sub> for increasing pressures up to 40 GPa. The diagrams evidence small amounts of Al metal as a secondary phase. At pressures above 2 GPa additional reflections are observed due to various phases of solid nitrogen. There are no indications for a pressure-induced structural phase transition in AlB<sub>2</sub> up to 40 GPa.

Lattice parameters as a function of pressure were determined from Rietveld-type fits of the diffraction diagrams. The compressibility of AlB<sub>2</sub> is moderately anisotropic as illustrated in Fig. 3(a) with the softer direction being parallel to the  $c$  axis. Up to 40 GPa, compression along  $c$  is 47% larger than along  $a$ . The  $c/a$  ratio decreases from 1.083 (0 GPa) to 1.060 at 40 GPa. From the lattice parameters we determine the unit cell volume as a function of pressure as shown in Fig. 3(b). The data are well represented by the Murnaghan relation<sup>29</sup>  $V(P) = V_0[(B'/B_0)P + 1]^{-1/B'}$ . With  $V_0 = 25.4734(5) \text{ \AA}^3$  fixed at the value determined from the zero-pressure data we obtain by least-squares fitting the bulk modulus  $B_0$  and its pressure derivative  $B'$  at zero pressure as listed in Table I.

Rietveld refinements of the crystal structure with the Al site occupation as a free parameter indicate that the sample studied here has an Al deficiency of  $\sim 11\%$ . This

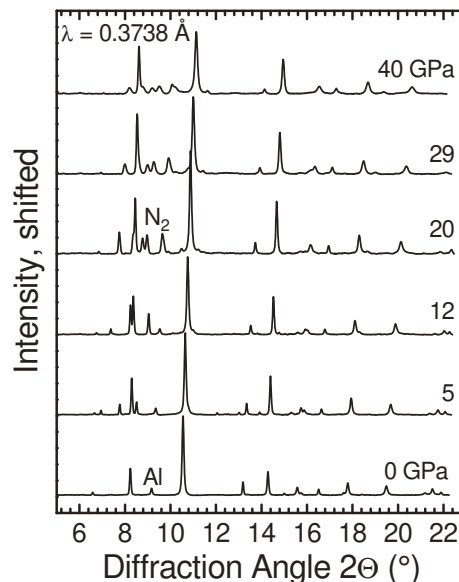


FIG. 2: X-ray powder diffraction diagrams of AlB<sub>2</sub> at various pressures ( $T = 298 \text{ K}$ ). ‘Al’ marks a peak due to fcc-Al. Additional peaks appear at pressures above 2 GPa due to various phases of solid nitrogen.

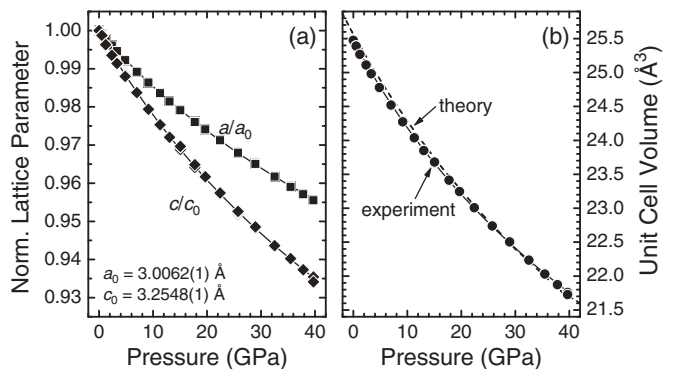


FIG. 3: (a) Experimental lattice parameters of AlB<sub>2</sub> as a function of pressure, normalized to their respective zero-pressure values. (b) Experimental (symbols and solid line) and calculated (dashed line) pressure-volume relations. The lines are given by the Murnaghan equation of state with the parameters listed in Table I.

is illustrated in Fig. 4 where difference curves for refinements of Al<sub>1.00</sub>B<sub>2</sub> and Al<sub>0.89</sub>B<sub>2</sub> are shown together with the experimental diffraction pattern. A Stephens peak profile<sup>31</sup> was used and a common isotropic thermal parameter for Al and B was optimized. The weighted profile  $R$  value (without background) reduces from  $R_{wp} = 8.5\%$  for Al<sub>1.00</sub>B<sub>2</sub> to  $R_{wp} = 6.9\%$  for Al<sub>0.89</sub>B<sub>2</sub>. This indication of substantial Al deficiency in AlB<sub>2</sub> is in agreement with density measurements<sup>25,26</sup> and recent single-crystal x-ray diffraction results.<sup>26</sup>

TABLE I: Structural parameters of  $\text{AlB}_2$  and  $\text{MgB}_2$ : zero-pressure volume  $V_0$  and lattice constants  $a_0, c_0$ ; bulk modulus  $B_0$ , and its pressure derivative  $B'$  at zero pressure. Variation of the  $c/a$  ratio with pressure is described by the quadratic polynomial  $c/a = c_0/a_0 + \alpha P + \beta P^2$  with the coefficients  $\alpha, \beta$  as listed below.

	$V_0$ ( $\text{\AA}^3$ )	$a_0$ ( $\text{\AA}$ )	$c_0$ ( $\text{\AA}$ )	$B_0$ (GPa)	$B'$	$c_0/a_0$	$\alpha$ ( $\text{GPa}^{-1}$ )	$\beta$ ( $\text{GPa}^{-2}$ )
$\text{AlB}_2$ , Exp. (300 K)	25.473(1)	3.0062(1)	3.2548(1)	170(1)	4.8(1)	1.0827(1)	$-8.8(1) \cdot 10^{-4}$	$0.77(4) \cdot 10^{-5}$
$\text{AlB}_2$ , Calc. (DFT/GGA)	25.565	2.9977	3.2855	176.8	3.64	1.096	$-12.0 \cdot 10^{-4}$	$1.09 \cdot 10^{-5}$
$\text{MgB}_2$ , Exp. (300 K) <sup>30</sup>	28.99(1)	3.0834(3)	3.5213(6)	147–155 <sup>a</sup>	(4.0) <sup>a</sup>			

<sup>a</sup> References 14,16,17 with the assumption that  $B' = 4$ .

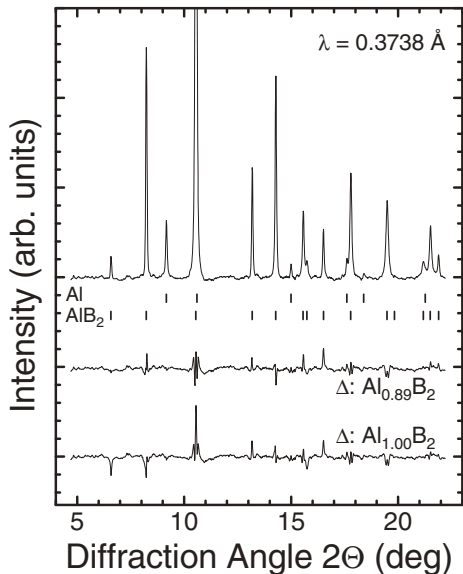


FIG. 4: X-ray powder diffraction diagram of  $\text{AlB}_2$  at 0 GPa and 293 K and difference curves ( $\Delta = I_{\text{exp}} - I_{\text{calc}}$ ) for refinements with and without Al-deficiency. Markers show peak positions due to  $\text{AlB}_2$  and fcc-Al.

### C. Raman spectra at ambient conditions

$\text{AlB}_2$  has one Raman-active zone-center phonon mode.<sup>32</sup> It is an in-plane vibration of the B atoms with  $E_{2g}$  symmetry, where neighboring B atoms move out of phase.<sup>19</sup> The powder sample we investigated contained some small shiny crystallites up to  $\sim 10 \mu\text{m}$  in size. Figure 5 shows Raman spectra recorded on two different crystallites and at a sample spot where no crystallites were discernible with an optical microscope. Besides a Lorentzian-shaped peak (FWHM of 40–50  $\text{cm}^{-1}$ ) which was attributed to the  $E_{2g}$  mode previously<sup>32</sup> we observe an additional step-like feature at the lower-energy side of the main peak. It is clearly visible in the single-crystal spectra and reduces to a weak shoulder in the powder spectrum. The powder spectrum resembles that reported by Bohnen *et al.*<sup>32</sup> The peak position of the  $E_{2g}$  mode of the two crystallites differs by 15  $\text{cm}^{-1}$  ( $\omega = 973$  and 988  $\text{cm}^{-1}$ ). In the powder spectrum the main peak occurs at an even lower energy of 952  $\text{cm}^{-1}$ . The step-like

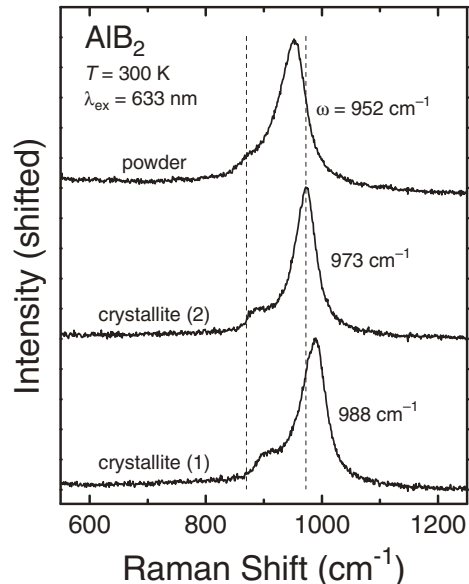


FIG. 5: Raman spectra of  $\text{AlB}_2$  at ambient conditions recorded on two crystallites and at a sample spot where no crystallites were discernible (‘powder’).

feature in the spectra of the crystallites shifts by the same amount as the main peak indicating that it is intrinsic to  $\text{AlB}_2$ . It appears likely that it is related to a peak in the calculated phonon density of states<sup>32</sup> which exists slightly below the energy of the  $E_{2g}$  mode.

### D. Raman spectra under pressure

Raman spectra of  $\text{AlB}_2$  were recorded for increasing pressures up to 25 GPa. Since the sample is somewhat deformed when pressure is applied and there seems to be some inhomogeneity of the powder, several spectra were collected at different locations of the sample. The spectra shown in Fig. 6(a) result from averaging about five spectra recorded at different spots that were selected for a narrow  $E_{2g}$  peak and low background. The zero-pressure frequency of the  $E_{2g}$  mode in these averaged diagrams amounts to 981(1)  $\text{cm}^{-1}$ . Two additional peaks near 875 and 1025  $\text{cm}^{-1}$  (at 0 GPa) are due to the methanol/ethanol pressure medium.

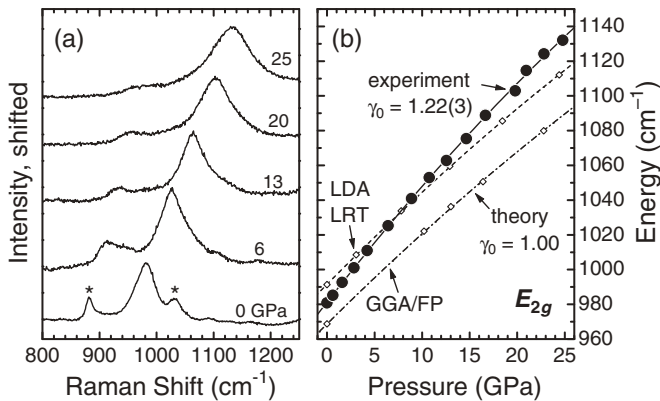


FIG. 6: (a) Raman spectra of  $\text{AlB}_2$  recorded for increasing pressures of 0–25 GPa ( $T = 300$  K). Peaks marked by asterisks are due to the methanol/ethanol pressure medium. (b) Experimental and calculated energies of the  $E_{2g}$  phonon mode. Experimental data are represented by circles and a solid line, results of the GGA/frozen-phonon and LDA/linear-response-theory calculations by a dash-dotted and dashed line, respectively. The lines represent quadratic functions fitted to the data.

The  $E_{2g}$  phonon frequency increases continuously with increasing pressure, but with slightly decreasing slope  $d\omega/dP$ . The zero-pressure mode-Grüneisen parameter amounts to  $\gamma_0 = 1.22(3)$  (based on  $B_0 = 170(1)$  GPa). Up to 10 GPa the peak width (FWHM) is essentially constant at  $44 \pm 2$   $\text{cm}^{-1}$  while at higher pressures it increases to  $\sim 90$   $\text{cm}^{-1}$  at 25 GPa. This is most likely related to the solidification of the pressure medium near 10 GPa. From the Raman data there are no indications for a structural phase transition.

### III. CALCULATIONS

#### A. Theoretical Method

The theoretical methods employed here were described in detail in the context of our recent work on  $\text{MgB}_2$ .<sup>19</sup> In summary, first-principles calculations of the total energy  $E_{tot}$  of the solid are the basis for the determination of the equation of state (EOS) and of the phonon frequencies. The energy is computed within the density functional theory (DFT) using a plane-wave basis and pseudopotentials.

For part of the actual calculations (equation of state and phonon frequencies in the *frozen-phonon approach*) we employed the VASP codes<sup>33,34,35,36</sup> within the generalized gradient approximation (GGA).<sup>37</sup> The ultrasoft Vanderbilt-type pseudopotentials<sup>38</sup> were supplied by Kresse and Hafner.<sup>39</sup> The pseudopotential for Al treats explicitly three valence electrons ( $3s^2 3p$ ); no semi-core states are included. A ‘harder’ variant of the potential was chosen and the nonlinear core correction<sup>40</sup> is applied in order to improve the transferability. The calculations

are carried out with a plane-wave cutoff energy of 23.6 Ry, and the Brillouin zone sampling is based on a  $\Gamma$ -centered  $16 \times 16 \times 16$  uniform mesh, yielding 270 to 1170  $k$ -points in the irreducible wedge of the Brillouin zone, depending on the symmetry of the lattice (equilibrium structure or crystal with the displacements of the  $E_{2g}(\Gamma)$  phonon). As the system is metallic, the  $k$ -space integration with the incompletely filled orbitals uses the tetrahedron method<sup>41</sup> with Blöchl’s corrections.<sup>42</sup>

Phonon frequencies were independently verified using the linear response theory<sup>43,44</sup> as implemented in the ABINIT package<sup>45</sup> within the local density approximation (LDA)<sup>46,47</sup> to the DFT. We used Hartwigsen-Goedecker-Hutter pseudopotentials<sup>48</sup> treating  $\text{Al}(3s^2 3p)$  and  $\text{B}(2s^2 2p)$  levels as valence states, a plane-wave cutoff of 60 Ry, and a  $12 \times 12 \times 12$   $k$ -point mesh. A Gaussian smearing with a broadening parameter of 0.04 Ry was applied to improve  $k$ -point sampling in the special points method. The structural parameters were optimized for each volume/pressure such that the stress tensor components  $\sigma_{xx}$  and  $\sigma_{zz}$  agreed within  $10^{-3}$  GPa.

#### B. Structural Properties

For fourteen unit cell volumes in the range 21.8–26.2  $\text{Å}^3$  we calculated (with the VASP codes) the total energy  $E(V)$  for different  $c/a$  values, thus determining the optimized structures  $[a(V), c(V)]$  and minimized total energies. The latter data were fitted by the Murnaghan relation for  $E(V)$ <sup>29</sup>

$$E(V) = E_0 + \frac{B_0 V_0}{B'} \left[ \frac{V}{V_0} + \frac{(V/V_0)^{1-B'} - B'}{B' - 1} \right] \quad (1)$$

which provided the static equilibrium volume  $V_0$  as well as the bulk modulus  $B_0$  and its pressure derivative  $B'$  at zero pressure. The structural parameters are summarized in Table I. The pressure–volume relation, shown in Fig. 3(b), compares well with the experimental data. The calculated equilibrium volume is 0.4% larger than the volume measured at 300 K. The individual lattice parameters are  $-0.3\%$  off the experiment for  $a_0$ ,  $+0.9\%$  for  $c_0$ , and consequently  $+1.2\%$  for  $c_0/a_0$ . The variation of  $c/a$  under pressure can be represented by a quadratic function and its coefficients are given in Table I.

#### C. Phonon frequencies

Energies of the  $E_{2g}$  phonon mode as a function of pressure were initially calculated in the frozen-phonon (FP) approach using the VASP codes and the GGA. For each phonon and pressure, the atoms are given six different displacements ranging from  $u/a = 0.005$  to 0.035 and the calculated energy values  $E(u)$  are fitted with a quartic polynomial. The resulting harmonic phonon frequencies and their respective pressure dependencies are listed in

Table II together with the experimental data for the  $E_{2g}$  mode and our previous FP-GGA results for  $\text{MgB}_2$ .<sup>19</sup> As illustrated in Fig. 6(b) the calculated zero-pressure frequency is only  $\sim 1\%$  lower than the experimental value, which is in the typical range for the difference between experiment and calculations of this type. Regarding the pressure dependence of the phonon frequency, however, we find an unusually large deviation of the theoretical results from the experiment. From the variation of the calculated phonon frequency with volume we obtain a zero-pressure mode-Grüneisen parameter of  $\gamma_0 = 1.00$  whereas the experimental value amounts to  $\gamma_0 = 1.22(3)$ .

Since the deviation of the theoretical results from the experimental data is larger than usual we performed a second calculation of the  $E_{2g}$  frequency under pressure using a rather different approach, namely linear-response-theory (LRT) in the LDA with the ABINIT package. Consistent with the common overestimation of bond strengths in the LDA we obtain here a somewhat larger zero-pressure phonon frequency, such that the two theoretical values bracket the experimental data at zero pressure. Over the whole pressure range the LDA/LRT calculation gives phonon frequencies which are consistently  $\sim 2.4\%$  larger than the corresponding GGA/FP results. Consequently, we obtain essentially the same pressure dependence  $d \ln \omega / dP$  for the two calculations. The deviation of the calculations from the experimental data is far beyond the typical uncertainty of such computations. The important difference between theory and experiment could be that the former is based on the ideal stoichiometry  $\text{Al}_1\text{B}_2$  whereas the real sample is Al deficient.

For comparison with previous calculations for  $\text{MgB}_2$  we have also calculated the frequency  $\omega$  of the  $B_{1g}$  phonon in  $\text{AlB}_2$  (out-plane motion of the boron atoms),<sup>19</sup> see Table II. The pressure dependence is characterized by a mode-Grüneisen parameter  $\gamma_0 = 1.06$ . In case of a constant, i.e., pressure-independent  $\gamma(V) \equiv \gamma_0$  the relation  $\omega(V) = \omega_0(V/V_0)^{-\gamma_0}$  holds. Thus, for both the  $E_{2g}$  and the  $B_{1g}$  mode in  $\text{AlB}_2$  with  $\gamma \approx 1$  there is a nearly inverse-proportional relation between the phonon frequency and volume. This is quite different from the situation in  $\text{MgB}_2$  where we do not only have the very large  $\gamma_0 = 2.5$  for the  $E_{2g}$  mode as noted before but also a rather small  $\gamma_0 = 0.6$  for the  $B_{1g}$  phonon (Table II).

The frozen phonon calculations also yield information on the anharmonicity of the phonon modes as described in the context of our  $\text{MgB}_2$  calculations.<sup>19</sup> In essence, the variation of the total energy with atomic displacement,  $E_{\text{tot}}(u)$ , can be represented by a polynomial where the ratio of the quartic to squared quadratic coefficients  $a_4/a_2^2$  is a measure of anharmonicity. In the harmonic limit  $a_4 = 0$ . For the  $E_{2g}$  mode in  $\text{AlB}_2$  we obtain  $|a_4/a_2^2| < 0.01 \text{ eV}^{-1}$  which is about three orders of magnitude lower than the corresponding values for  $\text{MgB}_2$  of  $a_4/a_2^2 = 4\text{--}8 \text{ eV}^{-1}$  (see Refs.19,23). Small anharmonicities are calculated for the  $B_{1g}$  modes of both compounds:  $a_4/a_2^2 = 0.27$  for  $\text{AlB}_2$  and  $a_4/a_2^2 = -0.05$  for  $\text{MgB}_2$ .

## IV. DISCUSSION

### A. Structural stability

In our x-ray diffraction and Raman experiments we do not find any indication for a structural phase transition or modulation of the structure. Group-subgroup symmetry considerations<sup>2</sup> indicate numerous possible distortions of the aristotype  $\text{AlB}_2$  most of which are realized in intermetallic compounds at ambient pressure. Pressure-induced structural phase transitions of  $\text{XY}_2$  intermetallic compounds have not been studied systematically. In the context of the  $\text{AlB}_2$  structure a number of rare-earth metal digallides,<sup>4,5,6,7</sup>  $\text{KHg}_2$ ,<sup>49</sup> and  $\text{LaCu}_2$ <sup>50</sup> were investigated at high pressures. From the available data a transition between the structure types  $\text{AlB}_2$  and  $\text{UHg}_2$  appears as a typical route. The  $\text{KHg}_2$  ( $\text{CeCu}_2$ ) structure type may occur as an intermediate phase.  $\text{AlB}_2$  and  $\text{UHg}_2$  are isopointal structures, distinguished only by their  $c/a$  ratios. Two clearly separated groups of compounds of  $\text{AlB}_2$  and  $\text{UHg}_2$  type are observed when plotting the  $c/a$  ratio versus ratio of the metallic radii of  $\text{XY}_2$  intermetallic compounds.<sup>6,51,52</sup> The  $\text{AlB}_2$  and  $\text{UHg}_2$  type branches are characterized by  $c/a$  ratios of 0.95–1.20 and 0.60–0.85, respectively. The compound  $\text{AlB}_2$  with  $c/a = 1.083$  (at 0 GPa) is located near the center of the former branch. In the pressure range to 40 GPa explored here it decreases only to 1.060. Pressures well above 1 Mbar may therefore be needed for a possible transition towards the  $\text{UHg}_2$  structure. At lower pressures a transition involving a buckling of the boron honeycomb layers may occur which could lead to phases of the  $\text{CeCu}_2$ ,  $\text{CeCd}_2$ , or  $\text{CaIn}_2$  type.<sup>2,6</sup>

### B. Raman spectra of $\text{AlB}_2$ vs. $\text{MgB}_2$

Raman spectroscopy is commonly applied to semiconductors and insulators but only to a much smaller extend to metals. It is essentially the group of elemental hcp metals that has been studied systematically, already in the late 1960s at ambient pressure<sup>53</sup> and more recently at high pressures (see e.g. Refs.54,55 and references therein). It may therefore be attributed to a lack of reference data that in case of  $\text{MgB}_2$  the observation of a very broad Raman feature (FWHM of  $\sim 300 \text{ cm}^{-1}$ ) near  $600 \text{ cm}^{-1}$  lead to a still unresolved controversy over the origin of this peak. It has initially been attributed<sup>32</sup> to the Raman-active  $E_{2g}$  mode which immediately raises the question of the large linewidth. The large peak width has been related to both strong electron phonon coupling and to structural disorder. The latter now appears less likely because Raman spectra of  $\text{MgB}_2$  powders are quite similar to those of recently available small single crystals<sup>56,57</sup> which are presumably less disordered. High-pressure Raman experiments<sup>19</sup> have cast doubt on the assignment to the  $E_{2g}$  phonon. They revealed a double-peak structure with peaks at  $603(6) \text{ cm}^{-1}$  and

TABLE II: Pressure and volume dependences of selected phonon frequencies of AlB<sub>2</sub> and MgB<sub>2</sub>. The zero pressure frequency  $\omega_0$  and the linear and quadratic pressure coefficients were obtained by least square fits of  $\omega(P) = \omega_0 + \alpha \cdot P + \beta \cdot P^2$  to the data. The theoretical mode Grüneisen parameters  $\gamma_0$  (at the theoretical equilibrium volume) are derived from a similar quadratic expression for  $\omega(V)$ .  $P$  has been obtained from  $V$  through the calculated  $P$ - $V$  relation (see text). The experimental mode Grüneisen parameter is determined from  $\omega(P)$  and the experimental  $P$ - $V$  relation.

Compound	Mode	$\omega_0$ (cm <sup>-1</sup> )	$\alpha$ (cm <sup>-1</sup> /GPa)	$\beta$ (cm <sup>-1</sup> /GPa <sup>2</sup> )	$\gamma_0$
AlB <sub>2</sub>	$E_{2g}$	969	5.425	-0.0235	1.00
	$E_{2g}$ (exp.)	981(1)	7.027	-0.0365	1.22(3)
	$B_{1g}$	490	2.968	-0.0087	1.06
MgB <sub>2</sub>	$E_{2g}$	535	8.974	-0.0780	2.5
	$B_{1g}$	695	3.065	-0.0190	0.6

750(20) cm<sup>-1</sup>. Neither of the two peaks could be attributed to the  $E_{2g}$  mode because of severe deviations from calculated phonon frequencies in terms of zero-pressure frequencies and/or the pressure dependences.

The present Raman data of AlB<sub>2</sub> show that it is possible to obtain Raman spectra with a well-defined  $E_{2g}$  peak from metallic samples of the AlB<sub>2</sub> structure. The difficulties encountered in case of MgB<sub>2</sub> are therefore not likely related to the metallicity of the sample nor intrinsic to the structure type. Crystallinity also appears to have only a small effect on the Raman spectrum as the Raman linewidth of the AlB<sub>2</sub> powder sample is comparable to that of the AlB<sub>2</sub> crystallites.

There are two properties of MgB<sub>2</sub> with regard to phonons which make it distinct from AlB<sub>2</sub>. First, the whole  $E_{2g}$  phonon branch along the  $\Gamma$ -A direction in the Brillouin zone exhibits very strong electron-phonon coupling in MgB<sub>2</sub>.<sup>23,58,59,60</sup> Second, the  $E_{2g}(\Gamma)$  mode shows pronounced anharmonicity.<sup>19,23</sup> Both electron-phonon and phonon-phonon interaction decrease the phonon lifetime and hence increase the phonon linewidth.<sup>61</sup> They are therefore the most likely causes for the absence of a well-defined  $E_{2g}$  Raman peak in MgB<sub>2</sub>.

### C. Metal deficiency in AlB<sub>2</sub>

Our x-ray diffraction data indicate an Al deficiency of 11% in AlB<sub>2</sub> in accord with previous density measurements and chemical analysis<sup>25,26</sup> as well as recent single-crystal x-ray diffraction results.<sup>26</sup> Although the change of the  $E_{2g}$  phonon frequency at different sample spots suggests that there is some variation of the Al content, there is no indication that growth of aluminum diboride in the composition Al<sub>1.0</sub>B<sub>2</sub> is possible. The occurrence of substantial metal deficiency appears to be common to many (transition) metal diborides.<sup>62</sup>

In case of AlB<sub>2</sub> this metal deficiency has important influence on the electronic structure. A comparison of the calculated bandstructures of AlB<sub>2</sub> and MgB<sub>2</sub> shows that the relative ordering and dispersions of the bands near the Fermi level are very similar. The difference between AlB<sub>2</sub> and MgB<sub>2</sub> can largely be treated in a rigid-band

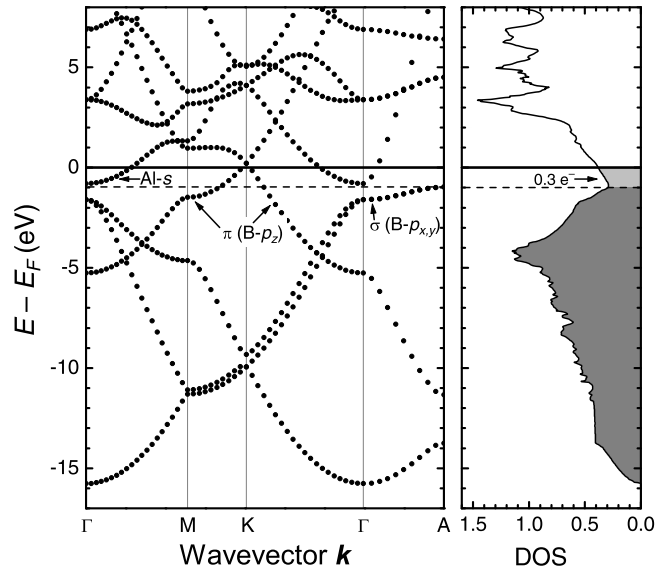


FIG. 7: Calculated electronic bandstructure and density of states (DOS) of AlB<sub>2</sub> at ambient pressure. Energies are given with respect to the Fermi energy  $E_F$ . The DOS is given in units of (states/eV/formula unit).

picture with a higher band filling for AlB<sub>2</sub>. It is therefore justified to discuss the observed Al deficiency of  $\sim 10\%$  in a rigid-band picture, too. Figure 7 shows the calculated electronic bandstructure<sup>63</sup> and density of states of AlB<sub>2</sub>. In case of the stoichiometric compound the  $\pi$ -type bands derived from boron  $p_z$  states and the bands with Al- $s$  character (near  $\Gamma$ ) are partially filled and give rise to the metallic state. 10% deficiency of Al removes 0.3 valence electrons and consequently lowers  $E_F$  by 0.9 eV which leads to a *complete depletion of the band with Al- $s$  character*. In other words, the experimentally observed Al deficiency is expected to lead to a qualitative change in the electronic structure compared to the ideal case of Al<sub>1</sub>B<sub>2</sub>. In terms of the Fermi surface this change means a removal of the electron pocket around  $\Gamma$ .

The measured mode-Grüneisen parameter of the Al<sub>0.9</sub>B<sub>2</sub> sample is  $\sim 20\%$  larger than calculated for Al<sub>1.0</sub>B<sub>2</sub>, a deviation which is far beyond the typical

uncertainty of such computations. The zero-pressure phonon frequency, on the other hand, seems to be hardly affected. The apparent difference between experiment and calculation is the Al deficiency of the sample which was not taken into account in the theory. We tentatively attribute the discrepancy between the experimental and calculated mode-Grüneisen parameters to the Al-deficiency-induced electronic changes discussed above. However, it cannot be excluded at this point that other effects are also at work. A more detailed analysis of the effect of Al deficiency on the electronic and lattice dynamical properties of AlB<sub>2</sub> is, however, beyond the scope of this work.

#### D. Metal deficiency in MgB<sub>2</sub>

Mg deficiency in MgB<sub>2</sub> was often indicated by the occurrence of MgO as a secondary phase in MgB<sub>2</sub> samples that were grown from a molar 1:2 mixture of Mg and B. Variations of  $T_c$  and even more of the pressure dependence of  $T_c$  for different samples appeared to be related to non-stoichiometry of the material. The correlation between composition, structural parameters and  $T_c$  has been established in an experiment by Indenbom *et al.*<sup>64</sup> By diffusion of Mg into a boron cylinder they produced a sample with a composition changing gradually between Mg<sub>1.0</sub>B<sub>2</sub> and Mg<sub>0.8</sub>B<sub>2</sub>. With decreasing Mg content the lattice parameter  $c$  increased by 0.003 Å (0.1%) and  $T_c$  increased from 37.2 to 39.0 K.

Tissen *et al.*<sup>12</sup> furthermore pointed out a correlation between the zero-pressure critical temperature  $T_{c,0}$  and the pressure derivative  $dT_c/dP$ : As  $T_{c,0}$  increases from 37.3 to 39.2 K for various samples,  $dT_c/dP$  changes from -2.0 to -1.1 K/GPa. Monteverde *et al.*<sup>9</sup> discussed a similar observation on a smaller number of samples in terms of the electronic band structure and band-filling effects related to the Mg non-stoichiometry. On the other hand, the pressure-induced changes of the electronic density of states calculated for MgB<sub>2</sub> are too small to account for the observed decrease of  $T_c$  under compression.<sup>20</sup> It is rather the increase in the relevant phonon frequencies which provides the main contribution to the pressure dependence of  $T_c$ .<sup>14,20,21</sup> It would therefore be rather surprising if electronic density effects – i.e., the electronic density  $N(E_F)$  at the Fermi level – were responsible for the large sensitivity of  $dT_c/dP$  on Mg non-stoichiometry.

The indications that Al deficiency in AlB<sub>2</sub> may affect the pressure dependence of the  $E_{2g}$  phonon frequency hints at an alternative possible explanation for the large sensitivity of  $dT_c/dP$  on Mg deficiency in MgB<sub>2</sub>. It was first pointed out by Yilderim *et al.*<sup>23</sup> that the  $E_{2g}$  phonon mode in MgB<sub>2</sub> exhibits a very large anharmonicity. Boeri *et al.*<sup>65</sup> showed theoretically that this effect arises in MgB<sub>2</sub> because here the Fermi level  $E_F$  is located only  $\sim 0.5$  eV below the top of  $\sigma$  bands of the equilibrium structure. The lattice distortion of the  $E_{2g}$  mode induces a splitting of these  $\sigma$  bands large enough that the lower

split-off band sinks completely below  $E_F$ .<sup>59,65</sup> This does not happen in AlB<sub>2</sub> and graphite, and anharmonicity is indeed negligible.

It is also noteworthy that the  $E_{2g}$  mode in AlB<sub>2</sub> is much higher in energy than the  $B_{1g}$  phonon whereas the reversed order is calculated for MgB<sub>2</sub> (see Table II) although both compounds are structurally quite similar. This effect was pointed out before and studied in Mg<sub>1-x</sub>Al<sub>x</sub>B<sub>2</sub> mixed crystals by Renker *et al.*<sup>66</sup> The interchange, which occurs only in undoped or moderately substituted material ( $0 < x < 0.2$ ), was also attributed to the electronic changes, especially the disappearance of the hole pockets from the Fermi surface for  $x > 0.2$ .

The metal content in MgB<sub>2</sub> affects the band filling, a larger Mg deficiency moving the Fermi level further below the top of the  $\sigma$  bands. It is therefore to be expected that the anharmonicity of the  $E_{2g}$  mode should decrease with decreasing Mg content. Lattice dynamical calculations showed that the  $E_{2g}$  anharmonicity decreases with increasing pressure<sup>19</sup> and the initially very large mode-Grüneisen parameter decreases too.<sup>19</sup> If the mode-Grüneisen parameters decreases as function of band filling at ambient pressure, i.e., due to non-stoichiometry of MgB<sub>2</sub>, it would, qualitatively, lead to the observed relation between  $dT_c/dP$  and Mg deficiency. This effect would be a manifestation of the changes of the lattice dynamics rather than changes of the electronic density of states. A more detailed and quantitative analysis is certainly needed, but the present results are indication of the importance of stoichiometry with regard to the superconducting properties of MgB<sub>2</sub>, specifically the pressure dependence of  $T_c$ .

#### V. CONCLUSIONS

We have studied the crystal structure of AlB<sub>2</sub> by x-ray powder diffraction to 40 GPa. The compressibility is moderately anisotropic consistent with the anisotropic bonding properties. In the pressure range studied here we did not observe a structural phase transition. Our x-ray diffraction data indicate an Al deficiency of  $\sim 11\%$  in agreement with previous reports. Despite the neglect of this non-stoichiometry in our first-principles calculations, the calculated structural properties are in good agreement with the experiment.

The  $E_{2g}$  zone-center phonon in metallic AlB<sub>2</sub> can be observed as a well-defined Raman peak. We conclude that the lack of such a Raman feature in MgB<sub>2</sub> is neither related to the metallicity or disorder of the sample nor is it a generic property of AlB<sub>2</sub>-type compounds. Our observations rather support the view that it is due to the strong electron-phonon coupling and/or anharmonicity which are distinct properties of MgB<sub>2</sub>. We found some deviation of the calculated pressure dependence of the  $E_{2g}$  phonon frequency of AlB<sub>2</sub> from the experimental data and tentatively attributed this to the Al deficiency of the AlB<sub>2</sub> sample which was not taken into account in

the theory.

Correlations between non-stoichiometry of MgB<sub>2</sub> and its superconducting properties have been pointed out previously. Here we considered possible effects of Mg deficiency in MgB<sub>2</sub> on its electronic structure and lattice dynamics. The anticipated changes are consistent with the available experimental data on the correlation between Mg content and the pressure dependence of  $T_c$ . This leads us to propose that the large variation of the pressure dependence of  $T_c$  (−0.7 to −2.0 K/GPa) in MgB<sub>2</sub> in various experiments may be caused by the effect of

non-stoichiometry on the lattice dynamics, mediated via changes in the electronic structure of MgB<sub>2</sub>.

### Acknowledgments

We thank Yu. Grin for calling our attention to the issue of the non-stoichiometry of AlB<sub>2</sub>. The computer resources used in this work were in part provided by the Scientific Committee of IDRIS, Orsay (France).

- 
- \* Electronic address: I.Loa@kf.mpg.de  
 † Permanent address: CNRS and Université P. et M. Curie, Laboratoire d'Optique des Solides UMR7601, T13 - C80, 4 pl. Jussieu, 75252 Paris - Cédex 05, France.
- 1 P. Villars and L. D. Calvert, *Persons's Handbook of Crystallographic Data for Intermetallic Phases* (American Society for Metals, Materials Park, OH 44073, 1991 & 1997), second Edition, 1991, and Desk Edition, 1997.
  - 2 R.-D. Hoffman and R. Pöttgen, *Z. Kristallogr.* **216**, 127 (2001).
  - 3 W. S. Williams, *JOM-J. Miner. Met. Mater. Soc.* **49**, 38 (1997).
  - 4 U. Schwarz *et al.*, *Z. Kristallogr.* **216**, 331 (2001).
  - 5 U. Schwarz *et al.*, *J. Alloys Comp.* **268**, 161 (1998).
  - 6 S. Bräuning, U. Schwarz, and K. Syassen (unpublished).
  - 7 U. Schwarz, S. Bräuning, Y. Grin, and K. Syassen, *J. Alloys Comp.* **245**, 23 (1996), *ibid.* **256**, 279 (1997).
  - 8 A. Saito *et al.*, *J. Phys.: Cond. Matter* **13**, L267 (2001).
  - 9 M. Monteverde *et al.*, *Science* **292**, 75 (2001).
  - 10 B. Lorenz, R. L. Meng, and C. W. Chu, *Phys. Rev. B* **64**, 012507 (2001).
  - 11 T. Tomita *et al.*, *Phys. Rev. B* **64**, 092505 (2001).
  - 12 V. G. Tissen, M. V. Nefedova, N. N. Kolesnikov, and M. P. Kulakov, *Physica C* **363**, 194 (2001).
  - 13 B. Lorenz, R. L. Meng, and C. W. Chu, cond-mat/0104303 (unpublished).
  - 14 T. Vogt *et al.*, *Phys. Rev. B* **63**, 220505 (2001).
  - 15 K. Prassides *et al.*, *Phys. Rev. B* **64**, 012509 (2001).
  - 16 J. D. Jorgensen, D. G. Hinks, and S. Short, *Phys. Rev. B* **63**, 224522 (2001).
  - 17 A. F. Goncharov *et al.*, *Phys. Rev. B* **64**, 100509 (2001).
  - 18 P. Bordet *et al.*, *Phys. Rev. B* **64**, 172502 (2001).
  - 19 K. Kunc *et al.*, *J. Phys.: Cond. Matter* **13**, 9945 (2001).
  - 20 I. Loa and K. Syassen, *Solid State Commun.* **118**, 279 (2001).
  - 21 X. J. Chen, H. Zhang, and H.-U. Habermeier, *Phys. Rev. B* **65**, 144514 (2002).
  - 22 S. Li-Ling *et al.*, *Chin. Phys. Lett.* **18**, 1401 (2001).
  - 23 T. Yildirim *et al.*, *Phys. Rev. Lett.* **87**, 037001 (2001).
  - 24 A. Y. Liu, I. I. Mazin, and J. Kortus, *Phys. Rev. Lett.* **87**, 087005 (2001).
  - 25 V. I. Matkovich, J. Economy, and R. F. Giese, Jr., *J. Am. Chem. Soc.* **84**, 2337 (1964).
  - 26 U. Burkhardt *et al.*, Annual Report 2000 of the Max-Planck-Institut für Chemische Physik fester Stoffe, Dresden, Germany.
  - 27 A. Hammersley, computer program FIT2D (ESRF, Grenoble), 1998.
  - 28 H. K. Mao, J. Xu, and P. M. Bell, *J. Geophys. Res.* **91**, 4673 (1986).
  - 29 F. D. Murnaghan, *Proc. Natl. Acad. Sci. U.S.A.* **30**, 244 (1944).
  - 30 M. E. Jones and R. E. Marsh, *J. Am. Chem. Soc.* **76**, 1434 (1954), ICSD Collection Code 26675.
  - 31 P. W. Stephens, *J. Appl. Cryst.* **32**, 281 (1999).
  - 32 K.-P. Bohnen, R. Heid, and B. Renker, *Phys. Rev. Lett.* **86**, 5771 (2001).
  - 33 G. Kresse and J. Hafner, *Phys. Rev. B* **47**, R558 (1993).
  - 34 G. Kresse, Ph.D. thesis, Technische Universität Wien, 1993.
  - 35 G. Kresse and J. Furthmüller, *Comput. Mat. Sci.* **6**, 15 (1996).
  - 36 G. Kresse and J. Furthmüller, *Phys. Rev. B* **54**, 11169 (1996).
  - 37 J. P. Perdew and Y. Wang, *Phys. Rev. B* **45**, 13244 (1992).
  - 38 D. Vanderbilt, *Phys. Rev. B* **41**, 7892 (1990).
  - 39 G. Kresse and J. Hafner, *J. Phys.: Cond. Matter* **6**, 8245 (1994).
  - 40 S. G. Louie, S. Froyen, and M. L. Cohen, *Phys. Rev. B* **26**, 1738 (1982).
  - 41 O. Jepsen and O. K. Andersen, *Solid State Commun.* **9**, 1763 (1971).
  - 42 P. E. Blöchl, O. Jepsen, and O. K. Andersen, *Phys. Rev. B* **49**, 16223 (1994).
  - 43 X. Gonze, *Phys. Rev. B* **55**, 10337 (1997).
  - 44 X. Gonze and C. Lee, *Phys. Rev. B* **55**, 10355 (1997).
  - 45 The ABINIT code is a common project of the Université Catholique de Louvain, Corning Incorporated, and other contributors (URL <http://www.abinit.org>). It relies on an efficient Fast Fourier Transform algorithm<sup>67</sup> for the conversion of wavefunctions between real and reciprocal space, on the adaptation to a fixed potential of the band-by-band conjugate gradient method<sup>68</sup> and on a potential-based conjugate-gradient algorithm for the determination of the self-consistent potential.<sup>69</sup>
  - 46 J. C. Slater, *Phys. Rev.* **81**, 385 (1951).
  - 47 W. Kohn and L. J. Sham, *Phys. Rev.* **140**, A1133 (1965).
  - 48 C. Hartwigsen, S. Goedecker, and J. Hutter, *Phys. Rev. B* **58**, 3641 (1998).
  - 49 H.-J. Beister, K. Syassen, H.-J. Deiseroth, and D. Toelstede, *Z. Naturforsch.* **48b**, 11 (1993).
  - 50 A. Lindbaum *et al.*, *J. Phys.: Cond. Matter* **12**, 3219 (2000).
  - 51 W. B. Pearson, *The Crystal Chemistry and Physics of Metals and Alloys* (Wiley Intersciences, New York, 1972).
  - 52 W. B. Pearson, *Proc. R. Soc. Lond.* **A365**, 523 (1979).

- <sup>53</sup> J. H. Parker, Jr., D. W. Feldman, and M. Ashkin, in *Light Scattering Spectra of Solids*, edited by G. B. Wright (Springer-Verlag, New York, 1969), pp. 389–397.
- <sup>54</sup> H. Olijnyk, A. P. Jephcoat, and K. Refson, *Europhys. Lett.* **53**, 504 (2001).
- <sup>55</sup> H. Olijnyk and A. Jephcoat, *Solid State Commun.* **115**, 335 (2000).
- <sup>56</sup> J. Hlinka *et al.*, *Phys. Rev. B* **64**, 140503 (2001).
- <sup>57</sup> H. Martinho *et al.*, cond-mat/0105204v4 (unpublished).
- <sup>58</sup> J. Kortus *et al.*, *Phys. Rev. Lett.* **86**, 4656 (2001).
- <sup>59</sup> J. M. An and W. E. Pickett, *Phys. Rev. Lett.* **86**, 4366 (2001).
- <sup>60</sup> Y. Kong, O. V. Dolgov, O. Jepsen, and O. K. Andersen, *Phys. Rev. B* **64**, 020501 (2001).
- <sup>61</sup> P. M. Rafailov, M. Dworzak, and C. Thomsen, *Solid State Commun.* **122**, 455 (2002).
- <sup>62</sup> A. M. Prokhorov, N. P. Lyakishev, G. S. Burkhanov, and V. A. Dement'ev, *Inorganic Materials* **32**, 1195 (1996), [*Neoganicheskie Materialy* **32**, 1365 (1996)].
- <sup>63</sup> The electronic bandstructure and density of states were calculated using the full-potential linearized augmented-plane-wave method method as implemented in the WIEN97 code.<sup>70</sup> For the exchange-correlation potential we employed the generalized gradient approximation of Ref.71. Scalar-relativistic corrections were included. The Al  $2p$  states were treated as band states using the local orbital extension of the LAPW method.<sup>70,72</sup> For  $k$ -point sampling employing the tetrahedron method, 296 points were used in the irreducible wedge of the Brillouin zone (4536 in total); other parameters were  $R_{\text{MT}} \cdot K_{\text{max}} = 8.0$ ;  $R_{\text{MT}} = 1.8$  and  $1.4 a_B$  for Al and B, respectively;  $l_{\text{max}} = 10$ ;  $G_{\text{max}} = 15$ .
- <sup>64</sup> M. V. Indenbom *et al.*, *JETP Letters* **74**, 274 (2001), [*Pis'ma v Zhurnal Éksperimental'noĭ i Teoreticheskoi Fiziki* **74**, 304 (2001)].
- <sup>65</sup> L. Boeri, G. B. Bachelet, E. Cappelluti, and L. Pietronero, cond-mat/0112075v1 (unpublished).
- <sup>66</sup> B. Renker *et al.*, *Phys. Rev. Lett.* **88**, 067001 (2002).
- <sup>67</sup> S. Goedecker, *SIAM J. on Scientific Computing* **18**, 1605 (1997).
- <sup>68</sup> M. Payne *et al.*, *Rev. Mod. Phys.* **64**, 1045 (1992).
- <sup>69</sup> X. Gonze, *Phys. Rev. B* **54**, 4383 (1996).
- <sup>70</sup> P. Blaha, K. Schwarz, and J. Luitz, *WIEN97, A Full Potential Linearized Augmented Plane Wave Package for Calculating Crystal Properties* (Karlheinz Schwarz, Techn. Universitt Wien, Austria, 1999), ISBN 3-9501031-0-4.
- <sup>71</sup> J. P. Perdew, S. Burke, and M. Ernzerhof, *Phys. Rev. Lett.* **77**, 3865 (1996).
- <sup>72</sup> D. Singh, *Phys. Rev. B* **43**, 6388 (1991).